

Multiscale Crystalline Structure of Confined Polypeptoid Films: The Effect of Alkyl Side Chain Branching

Q. Wang, R. Li

To be published in "ACS Macro Letters"

August 2022

Photon Sciences

Brookhaven National Laboratory

U.S. Department of Energy

USDOE Office of Science (SC), Basic Energy Sciences (BES) (SC-22)

Notice: This manuscript has been authored by employees of Brookhaven Science Associates, LLC under Contract No. DE-SC0012704 with the U.S. Department of Energy. The publisher by accepting the manuscript for publication acknowledges that the United States Government retains a non-exclusive, paid-up, irrevocable, world-wide license to publish or reproduce the published form of this manuscript, or allow others to do so, for United States Government purposes.

DISCLAIMER

This report was prepared as an account of work sponsored by an agency of the United States Government. Neither the United States Government nor any agency thereof, nor any of their employees, nor any of their contractors, subcontractors, or their employees, makes any warranty, express or implied, or assumes any legal liability or responsibility for the accuracy, completeness, or any third party's use or the results of such use of any information, apparatus, product, or process disclosed, or represents that its use would not infringe privately owned rights. Reference herein to any specific commercial product, process, or service by trade name, trademark, manufacturer, or otherwise, does not necessarily constitute or imply its endorsement, recommendation, or favoring by the United States Government or any agency thereof or its contractors or subcontractors. The views and opinions of authors expressed herein do not necessarily state or reflect those of the United States Government or any agency thereof.

Multiscale Crystalline Structure of Confined Polypeptoid Films: The Effect of Alkyl Side Chain Branching

Qi Wang,¹ Liying Kang,¹ Xiangyu Xu,¹ Meng Zhang,² Albert Chao,² Jianxia Chen,¹ Zhijing Han,¹ Huihui Yu,¹ Ruipeng Li,³ Yixin Zhao,⁴ Donghui Zhang^{2*} and Naisheng Jiang^{1*}

¹ School of Materials Science and Engineering, University of Science and Technology Beijing, Beijing 100083, China

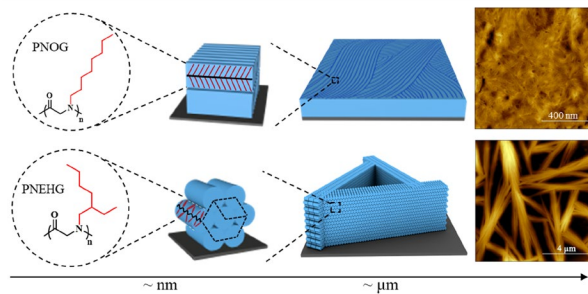
² Department of Chemistry, Louisiana State University, Baton Rouge, Louisiana 70803, United States

³ National Synchrotron Light Source II, Brookhaven National Laboratory, Upton, New York 11973, United States

⁴ Beijing Key Laboratory for Precise Mining of Intergrown Energy and Resources, China University of Mining and Technology, Beijing, 100083, China

Corresponding to: naishengjiang@ustb.edu.cn and dhzhang@lsu.edu

For Table of Contents use only



Abstract

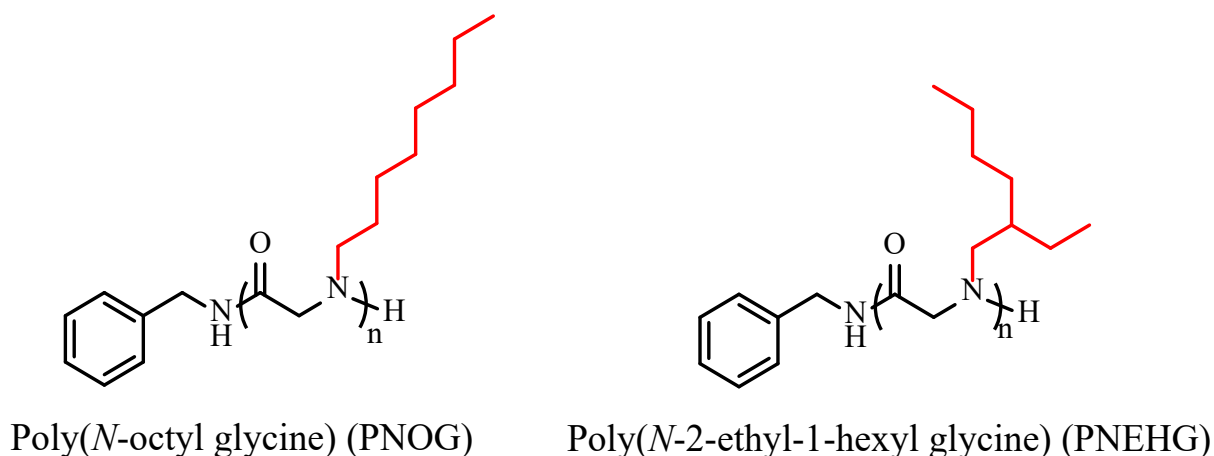
We report the effect of alkyl side chain branching on melt-recrystallization of nanoconfined polypeptoid films using poly(*N*-octyl glycine) (PNOG) and poly(*N*-2-ethyl-1-hexyl glycine) (PNEHG) as model systems. Upon cooling from the isotropic melt, confined PNOG molecules recrystallize into near-perfect orthorhombic crystal structure with the board-like molecules stacked face-to-face in the substrate-parallel direction, resulting in long-range ordered wormlike lamellae that occupy the entire film. By contrast, rod-like PNEHG molecules bearing branched *N*-2-ethyl-1-hexyl side chains stack into a columnar hexagonal mesophase with their backbones oriented parallel to the substrates, forming micron sized sheaf-like superstructures under confinement, exposing large areas of empty spaces in the film. These findings highlight the effect of alkyl side chain branching on the packing motif and multiscale crystalline structure of polypeptoids under nanoconfined geometry.

Crystallization of macromolecules is a fascinating process that produces multiscale hierarchical structures with chains orderly packed together into lamella, stacked lamellae and complex superstructures, such as spherulites.¹ Among various systems, the crystallization behavior of ultrathin polymer films has attracted special attention due to the emerging of polymer-based nanotechnologies, such as functional coatings, microelectronics and photovoltaic devices.^{2, 3} Interestingly, molecular orientation, crystalline morphology, nucleation and growth behavior of ultrathin polymers films can deviate significantly from their bulk counterparts due to the so-called “nanoconfinement effect”.³⁻⁸ Since mechanical, optical and electrical properties of polymeric materials are directly linked to their crystalline structure, understanding and controlling the crystallization of nanoconfined polymer films are essential to achieve desired performance. Apart from applicational demands, confined crystallization also offers an opportunity to gain a better understanding of the crystalline behavior of a particular polymer, where crystals often display anisotropic behaviors and quasi-two-dimensional morphologies that can be characterized by various experimental techniques.^{3, 9}

Polypeptoids, a family of synthetic peptidomimetic polymers, have recently attracted much attention due to their potential for biotechnological applications, such as antifouling coatings,¹⁰⁻¹² drug/gene delivery^{13, 14} and biosensing.¹⁵⁻¹⁷ Differs from polypeptides, polypeptoids lack hydrogen bonding interactions and stereogenic centers along the backbone, allowing their molecular packing and phase behavior to be systematically tailored by adjusting the *N*-substituent structures.^{18, 19} Crystallization and crystallization-driven self-assembly of polypeptoids have attracted growing interests due to their capability to form a variety of well-defined nanostructures, including nanofibers,²⁰⁻²² nanotubes,²³ nanosheets²⁴⁻²⁶ and more sophisticated hierarchical structures.^{25, 27} It has been found that polypeptoids with relatively long *n*-alkyl side chains are crystallizable and exhibit two ordered phases, a highly ordered orthorhombic crystalline phase and a “sanidic” liquid crystalline (LC) mesophase, upon cooling from the isotropic melt.^{28, 29} The two corresponding transition temperatures are strongly coupled, suggesting a correlation between main chain and side chain packings.²⁸ In the crystalline phase, the polypeptoids chain adopt a board-like structure where the backbone is fully extended in predominantly *cis*-amide conformation and is approximately coplanar with the linear *n*-alkyl side chains (Figure S1).³⁰ Interestingly, when the long alkyl side

groups are asymmetrically branched, *e.g.*, in the case of racemic *N*-2-ethyl-1-hexyl side chains, the polymer shows a single first-order transition with a small enthalpic change upon cooling from isotropic melt and prefers to stacked hexagonally into an LC mesophase.^{25, 28} The asymmetrical branching of alkyl side chains also has a significant impact on the solution aggregate morphology of amphiphilic coil-crystalline diblock copolypeptoids, producing symmetrical hexagonal nanosheets in dilute solution.²⁵ However, despite many interesting findings, the hierarchical self-assembly of crystallizable polypeptoid homopolymers is not fully understood. How alkyl side chain branching affects the crystallization of polypeptoids under confined geometry also remains unclear.

Scheme 1. Chemical structures of PNOG and PNEHG



In this study, two polypeptoids, *i.e.*, poly(*N*-octyl glycine) (PNOG) bearing linear *n*-octyl side chains and poly(*N*-2-ethyl-1-hexyl glycine) (PNEHG) bearing branched racemic *N*-2-ethyl-1-hexyl side chains were synthesized to investigate the effect of side chain branching on their melt-recrystallization in the thin films (Scheme 1) (PNOG: $DP_n = 43$, $M_n = 7.3$ kg/mol, $\bar{D} = 1.17$; PNEHG: $DP_n = 54$, $M_n = 9.2$ kg/mol, $\bar{D} = 1.10$ (Table S1 and Figure S2-S4)). Based on differential scanning calorimetry (DSC), the isotropic melting temperatures (T_m) for PNOG and PNEHG bulk samples were determined to be 177.5 °C ($\Delta H_{m, 2} = 41.3$ J/g) and 156.3 °C ($\Delta H_m = 3.9$ J/g), respectively (Figure S5). During the cooling cycle, the bulk PNOG shows an isotropic melt to “sanidic” LC mesophase transition at $T_{LC} = 144.1$ °C and a LC mesophase to crystalline phase transition at $T_C = 24.6$ °C, respectively.^{28, 29} By contrast, PNEHG exhibit only one weak exothermic peak at $T_{LC} = 134.2$ °C during the cooling cycle (Figure S5), corresponding to the transition from isotropic melt to columnar hexagonal LC mesophase (*vide infra*). Similar thermal behaviors were also found for

PNOG and PNEHG with higher DP_n (Figure S5), implying the effect of side chain branching on phase transition is not sensitively dependent on the M_w . Ultrathin films of PNOG and PNEHG with the thickness of *ca.* 50 nm were spin-coated onto HF-treated silicon (Si) substrates and subjected to melt-recrystallization process. After thermally annealed at $T = 200\text{ }^\circ\text{C} \gg T_m$ for 1 h, two types of cooling procedures were applied subsequently: (1) slowly cooled to room temperature (RT $\sim 22\text{ }^\circ\text{C}$) over a period of 13 h, resulting in a non-isothermal crystallization process (Figure S6);³¹ (2) rapidly cooled to RT at a rate of $\sim 200\text{ }^\circ\text{C}/\text{min}$, then kept at RT isothermally to induce recrystallization. The thickness and internal structure of the films were further characterized by specular X-ray reflectivity (XRR) (Figure S7). The detailed synthesis of the polymers, polymer characterization, thin film preparation and characterization were summarized in the Supporting Information (SI) section.

In situ, high temperature grazing incident wide-angle X-ray diffraction (GIWAXD) experiments were performed to investigate the structure and phase transition of PNOG and PNEHG thin films. At $T \gg T_m$ (*i.e.*, $T = 200\text{ }^\circ\text{C}$), both PNOG and PNEHG films show amorphous halo rings in GIWAXD (Figure S8), suggesting both polymers are fully disordered and randomly oriented in the molten state. The phase transition temperatures (*i.e.*, T_{LC} or T_C) of PNOG and PNEHG films upon cooling are estimated by the peak intensity and position changes in the temperature-dependent GIWAXD profiles (Figure S9). Upon transition from isotropic melt to LC mesophase, PNEHG film show less pronounced changes in the molecular distance separated by *N*-alkyl side chains ($\sim 0.1\text{ nm}$) compared to the PNOG counterpart ($\sim 0.4\text{ nm}$) (Figure S9), consistent with the weaker exothermic peak in DSC. Along with the DSC results, it was found that the T_{LC} and T_C values of the 50 nm-thick PNOG film remain almost unchanged as compared to those of the bulk counterpart, while the PNEHG film shows a $\sim 20\text{ }^\circ\text{C}$ T_{LC} reduction relative to bulk (see SI for detailed explanation).

After slowly cooling the sample to RT (*i.e.*, $T = \sim 22\text{ }^\circ\text{C} < T_C$), the recrystallized PNOG film shows a series of well-defined arc-shaped (00*l*) reflections located at $q = 0.30, 0.60, 0.90, 1.20$ and 1.50 \AA^{-1} in the out-of-plane (q_z) direction (Figure 1a), corresponding to long-range ordered side-by-side molecular packing of PNOG (separated by *n*-octyl side chains) along the crystallographic *c*-axis.^{25, 26, 28, 30} The characteristic (100) reflection at $q = 1.39\text{ \AA}^{-1}$ in the in-plane (q_{xy}) direction corresponds to the face-to-face molecular packing along the crystallographic *a*-axis ($d = 0.45\text{ nm}$).

The well-defined $(10l)$ reflections located along the perpendicular direction of q_{xy} -axis suggest a long-range correlation between face-to-face and side-by-side packings.^{29, 30} The off-axis reflection located at $q = 1.33 \text{ \AA}^{-1}$ ($d = 0.47 \text{ nm}$) with an angle of $\sim 27^\circ$ with respect to the q_{xy} direction (Figure S10) was assigned to the distance between the closely packed n -octyl side chains within the typical V-shaped motifs with n -octyl side chains splaying on both sides of the backbone.^{24, 30} The non-isotropic diffraction pattern indicates that the crystalline orientation is preferential “edge-on” (Figure 2a), allowing n -octyl side chain ends to maximize their contacts with the HF-treated Si surface. This is consistent with poly(N-decylglycine) films prepared on hydrophobic Si,³² where the board-like molecules are stacked side-by-side in the substrate-normal direction to lower the interfacial energy at both free surface and polymer-substrate interface.

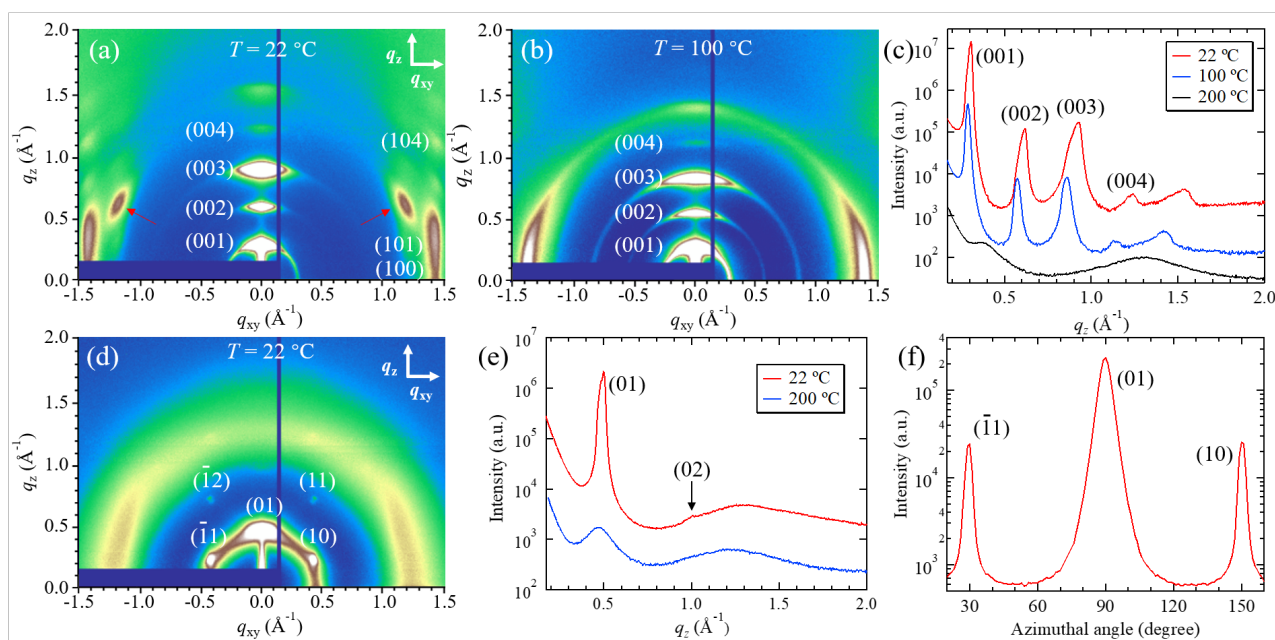


Figure 1. 2D GIWAXD images of the 50 nm-thick PNOG films measured at (a) RT ($T < T_C$) and (b) 100 °C ($T_C < T < T_{LC}$), respectively. The out-of-plane (q_z) and in-plane (q_{xy}) directions are indicated by arrows. The peaks attributed to the distance between the closely packed n -octyl side chains are indicated by the red arrows in (a). The corresponding 1D GIWAXD profiles along the q_z direction were shown in (c). Also shown are 2D GIWAXD image of the 50 nm-thick PNEHG films measured at RT (d), the corresponding 1D GIWAXD profile along the q_z direction measured at $T = 22$ and 200 °C (e), and the azimuthal profile of 2D GIWAXS patterns of PNEHG films measured at RT at $q = 0.49 \text{ \AA}^{-1}$ (f). Note that the 1D GIWAXD intensity data in (c) and (e) have been shifted vertically for clarity.

When the film is recrystallized at temperatures below T_{LC} but above T_C , *i.e.*, within the “sanidic” LC mesophase, the PNOG molecules are more randomly oriented inside the film, which give a series of azimuthal rings of $(00l)$ reflections (Figure 1b). While the majority of molecules are still edge-on,

a lack of long-range correlation between face-to-face and side-by-side packings is evidenced by the absence of higher order ($10l$) reflections, likely arising from the disordered planes of molecules along a -axis (Figure S11).²⁹ Importantly, the off-axis peaks corresponding to the n -octyl side chain packing also disappeared, indicating the disordering of side chains in the mesophase. The ($00l$) peaks along q_z at 100 °C (*i.e.*, $T_C < T < T_{LC}$) are also less intense than those measured at RT (Figure 1c). By using the Scherrer equation,^{32, 33} the structural coherence of (001) is estimated to be 27.6 nm and 22.4 nm at RT and 100 °C, respectively, suggesting a more ordered side-by-side packing in the crystalline phase relative to the LC mesophase.

Figure 1d displays the 2D GIWAXD pattern of the recrystallized PNEHG film measured at $T = 22$ °C after slow cooling process. The pattern clearly indicates that PNEHG molecules are hexagonally packed: Apart from the (01) peak located at $q_z = 0.49 \text{ \AA}^{-1}$ ($d = 1.28 \text{ nm}$), which corresponds to the distance between adjacent PNEHG separated by N -2-ethyl-1-hexyl sidechains (1.47 nm) in an interdigitated arrangement,²⁸ there are two off-axis diffraction spots with an angle of 60° respect to the q_z direction (Figure 1d and 1f), corresponding to the (10) and ($\bar{1}1$) reflections in the hexagonal lattice.³⁴⁻³⁶ Multiple weakly scattered peaks correspond to higher order reflections are also discernible. Hence, the PNEHG molecules, having their bulky side chains radially and outwardly displayed along the extended backbone due to steric hindrance,²⁵ are rod-like and packed into a columnar hexagonal (Col_{hex}) mesophase in the substrate-normal direction with their backbone or the molecular director (n) oriented parallel to the substrate (Figure 2b). Unlike the board-like PNOG molecules with their backbone being nearly coplanar with the n -octyl side chains, the asymmetric branching of the 2-ethyl-hexyl side chains imposes a much greater steric hindrance, rendering PNEHG molecules adopt a rod-like geometry with the side chain splaying out along an extended backbone. Two diffuse arcs with intensity maxima located at $q = 1.28 \text{ \AA}^{-1}$ are also discernible, likely arising from the average distance between relatively disordered N -2-ethyl-1-hexyl side chains (0.49 nm).³⁰ Hence, the molecular packing of polypeptoid thin films is significantly altered when the alkyl side chains are asymmetrically branched. This is in stark contrast to the very similar molecular packing of poly(3-(2'-ethyl)hexylthiophene) and poly(3-hexylthiophene) into lamellar-like mesophase irrespective of their difference in the sidechain branching pattern.³⁷⁻³⁹ Nevertheless, it is

consistent with poly(9,9-bis(*n*-octyl)fluorene-2,7-diyl) and poly(9,9-bis(2-ethylhexyl)fluorene-2,7-diyl) where asymmetric sidechain branching gives rise to different molecular packing motifs.^{35, 40} The seemingly contradictory effects of alkyl side chain branching may have to do with the difference in the structural coupling between side chain and main chain packing in different polymer systems.

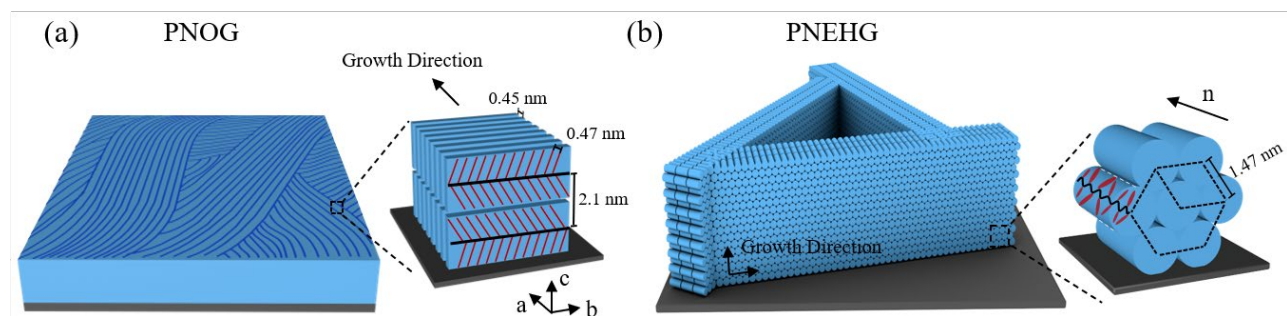


Figure 2. Schematic illustrations of the molecular packing and hierarchical crystalline structure of (a) PNOG and (b) PNEHG thin films on solid substrates.

The formation of crystalline lamellae of PNOG and PNEHG films induced by melt-recrystallization was further characterized by AFM and GISAXS. Note that the non-annealed as-cast films are relatively homogeneous and featureless with surface roughness less than 1.2 nm, as confirmed by XRR (Figure S7) and AFM (Figure S12). As seen from Figure 3a, the PNOG film recrystallized from slow cooling is occupied by well-organized long wormlike crystalline lamellae that run parallel to the surface. Since crystal growth of long PNOG chains along the backbone direction (*i.e.*, *b*-axis) is less favorable due to potential effects of chain ends and polymer dispersity, it is reasonable that the *b*-axis crystalline dimension corresponds to the width of the long worms. Along with GIWAXD results, molecular arrangement inside of these wormlike structures can be rationalized: While the board-like PNOG molecules are stacked side-by-side (along *c*-axis) in the substrate-normal direction, the elongation of the long wormlike crystalline lamellae in the lateral direction is attributed to the face-to-face stacking of PNOG along *a*-axis (Figure 2a). The GISAXS result of the slowly cooled sample measured at RT shows a broad peak maximized at 0.048 \AA^{-1} along q_{xy} (Figure 3e), corresponding to the long period,⁴¹ *i.e.*, the d-spacing between adjacent crystalline lamellae, which is in good agreement with the AFM result (Figure 3a). This long period is almost identical to the theoretical value of the fully extended backbone length of PNOG (12.9 nm),³⁰ suggesting the PNOG molecules are likely unfolded (*i.e.*, fully extended) in the crystalline state.

The question then arises: In what state did the well-organized wormlike crystalline lamellae of PNOG form? Based on high-temperature GISAXS (Figure 3e), the broad peak attributed to the long period, *i.e.*, the spacing between adjacent crystalline lamellae, begins to appear after cooling to 150 °C, indicating the crystalline lamellae have already formed upon the transition from isotropic melt to “sanidic” LC mesophase. However, the peaks that correspond to long periods in the LC mesophase are much less intense compared to those observed in the crystalline state. Further cooling to $T < T_C$ induces the formation of a well-defined long period, attributing to the enhanced structural ordering and long-range correlation between the crystalline planes at the molecular level.

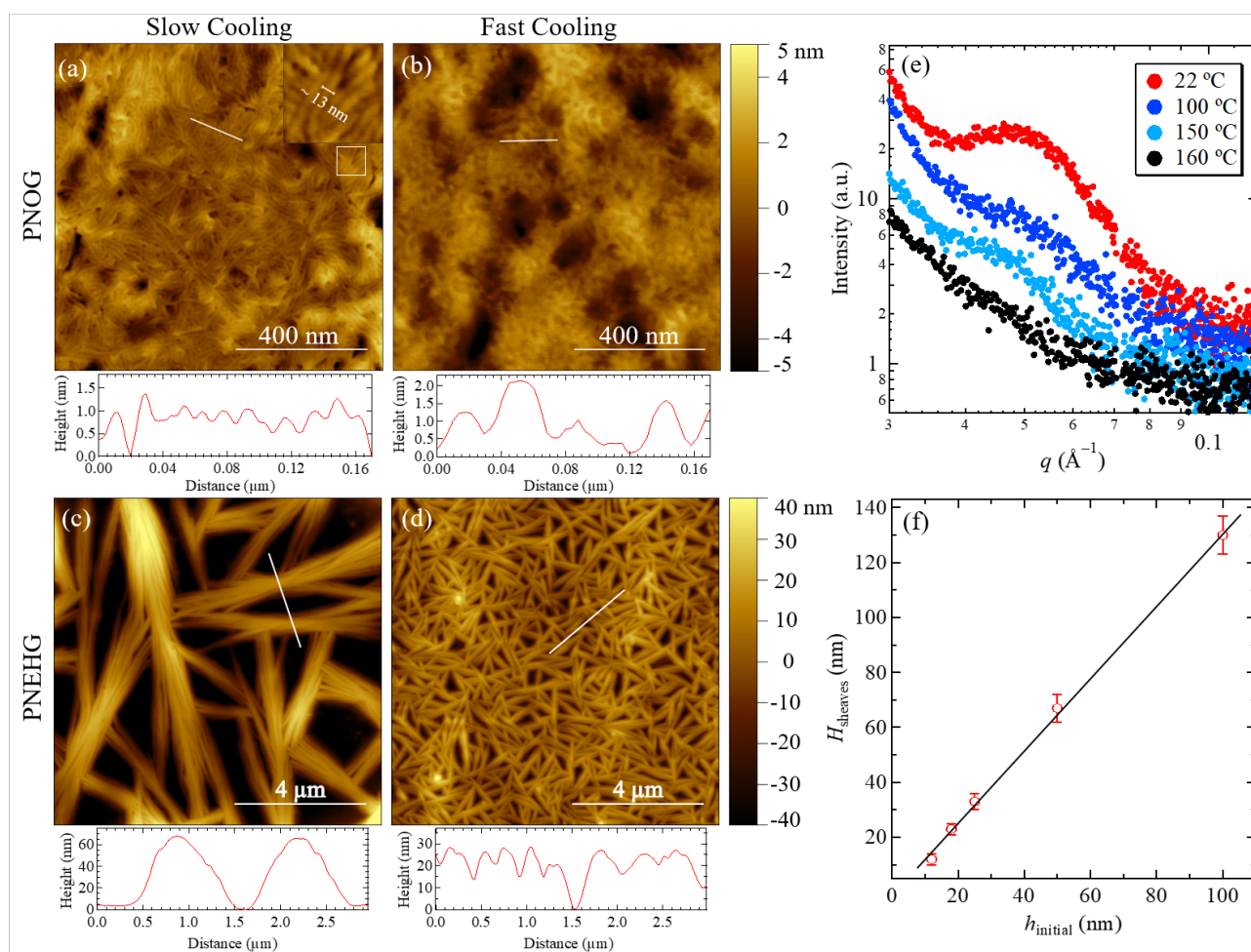


Figure 3. Representative AFM height images of PNOG (top row) and PNEHG (bottom row) films that recrystallized from isotropic melt via slow cooling (a and c) and fast cooling (b and d). The magnified view of the region indicated by the white square is shown in the inset of (a). The cross-sectional height profiles along the white lines are shown below each image. (e) *In situ* high-temperature 1D GISAXS profiles for the PNOG films along q_{xy} during the cooling process. The intensity data were shifted vertically for clarity. (f) The average height of the sheaves (H_{sheaves}) as function of the initial film thickness (h_{initial}) of PNEHG. The black solid line corresponds to the best fit to the h_{initial} dependence of H_{sheaves} using a linear function of $H_{\text{sheaves}} =$

$1.3h_{\text{initial}}$.

The hierarchical lamellar morphology upon recrystallization becomes vastly different when the alkyl side chains are asymmetrically branched. It was found that the columnar hexagonally packed PNEHG molecules grow into large sheaf-like structures consisting of dozens of rigid fibrous lamellae with an average width of ~ 100 nm for each fiber (Figure 3c and Figure S13). The crystalline morphology of PNEHG is reminiscent of the so-called axialite or hedrite,^{1, 42} a superstructure comprised of multilayer crystalline lamellae that spread out from a growth center. Interestingly, unlike the wormlike PNOG lamellae that are densely packed throughout the entire film, the PNEHG lamellae grew to a much greater height than the initial thickness of the as-cast film (h_{initial}), leaving behind microscopic holes in the film due to the consumption of amorphous materials. The identical sheaf-like morphology was observed by recrystallization of PNEHG films via slow cooling with varying initial thickness ($20 \text{ nm} \leq h_{\text{initial}} \leq 100 \text{ nm}$) (Figure S14). The average height of sheaves (H_{sheaves}) is found to be ~ 30 % greater than h_{initial} (*i.e.*, $H_{\text{sheaves}} = 1.3h_{\text{initial}}$) (Figure 3f). Since the rod-like PNEHG molecules are preferentially “lying-down” with n aligned parallel to the substrate, we conclude that the lamellar faces are determined by the 2D growth of PNEHG crystals with a Col_{hex} lattice, while the width is attributed to the end-to-end stacking of PNEHG along the backbone direction (Figure 2b). Unlike the symmetric hexagonal sheet formation previously found in the solution self-assembly of PNMG-*b*-PNEHG diblock copolypeptoids,²⁵ the lamellar growth of PNEHG films are highly asymmetric: While lateral stacking of the rod-like PNEHG molecules can reach up to several microns before colliding with another crystalline sheaf, the molecular stacking in the substrate-normal direction is much limited, resulting in average thickness of several tens of nanometers in for the fibrous lamellae. This indicates that the anisotropic lamellar growth is largely suppressed in the substrate-normal direction, where transportation of PNEHG molecules towards the liquid crystal growth front become increasingly retarded when the lamellae grow higher than h_{initial} and eventually halted at $H_{\text{sheaves}} = 1.3h_{\text{initial}}$.

The final crystalline morphology of PNOG and PNEHG films highly depends on the cooling conditions. At molecular level, it was found that the fast cooled film exhibits similar molecular packing and crystalline ordering relative to the slowly cooled counterpart (Figure S15). While at

microscale, rapid cooling leads to the formation of shorter wormlike structures of PNOG that appear to be less densely packed in the film relative to those formed under slow cooling condition (Figure 3b). We postulate that rapid quenching with a large degree of supercooling increases the nuclei density and accelerates crystal growth, resulting in less long-range ordered lamellar stacks. Similarly, when fast cooling was applied to the PNEHG film, the areal density of the sheaf-like structure was notably increased, and the average size of the sheaves became smaller than those observed in slowly cooled samples (Figure 3d). These findings indicate that the melt-recrystallization for both PNOG and PNEHG is governed by nucleation and growth processes.

In conclusion, we investigated the confined melt-crystallization of polypeptoids bearing two different alkyl side chain architectures, *i.e.*, linear *vs.* branched. With long linear alkyl side chains, PNOG molecules form highly crystalline thin films with densely packed wormlike lamellar crystals on hydrophobic silicon substrates. The crystalline films are anisotropic with the board-shaped PNOG molecules packed into orthorhombic lattice and preferentially stacked edge-on in the substrate-normal direction. By contrast, PNEHG molecules bearing branched *N*-2-ethyl-1-hexyl side chains stack into a Col_{hex} mesophase with the molecular director (*n*) aligned parallel to the substrate when recrystallized from isotropic melt. This results in the formation of hierarchically ordered sheaf-like superstructures constituted of stacked fibrous PNEHG lamellae, exposing large areas of empty spaces in the substrate-supported films. Supercooling conditions were shown to strongly influence the nanostructured morphologies of the films, consistent with the recrystallization of both PNOG and PNEHG films occurring by nucleation and growth processes. These findings shed new light on the relationships among side chain architecture, molecular packing motif and multiscale crystalline structure of polypeptoids under nanoconfined geometry. This study also demonstrates that side chain branching can serve as an effective approach for controlling the hierarchical assembly of crystallizable polymers. Investigations on the effects of molecular weight and polymer-substrate interaction are currently in progress for a more comprehensive understanding of confined crystallization of polypeptoids bearing long alkyl side chains.

Conflicts of interest

The authors declare no competing financial interest.

Associated content

Supporting Information

The Supporting Information is available free of charge on the ACS Publications website at DOI: [http: www.acs.org](http://www.acs.org).

Experimental Section, general crystalline packing of polypeptoid bearing linear alkyl side chains, ¹H NMR spectra, SEC-dRI chromatograms and DSC thermograms of PNOG and PNEHG polymers, the temperature change as a function of time during the slow cooling process, XRR analysis of the PNOG and PNEHG films, *in situ* high-temperature GIWAXD results of PNOG and PNEHG thin films, illustration of the PNOG molecular packing in LC mesophase, additional AFM and GIWAXD results of the as-cast and recrystallized films with different thickness and cooling process.

Acknowledgment

The authors thank Prof. Yue Zhang (USTB) for the access to AFM, Dr. Masafumi Fukuto (NSLS-II) and Dr. Yu Chen (BSRF) for assisting the synchrotron X-ray scattering measurements. The work was supported by the National Natural Science Foundation of China (52073025), the National Science Foundation (CHE 1609447 and 2003458) and the Fundamental Research Funds for the Central Universities (FRF-IDRY-20-003, Interdisciplinary Research Project for Young Teachers of USTB). This research used the Complex Materials Scattering (CMS/11-BM) beamline, operated by the National Synchrotron Light Source II at Brookhaven National Laboratory, which is supported by the U.S. Department of Energy, Office of Science, Office of Basic Energy Sciences, under Contract No. DE-SC0012704. This work was also carried out with the support of 1W1A Diffuse X-ray Scattering Station, Beijing Synchrotron Radiation Facility (BSRF).

References

- (1) Crist, B.; Schultz, J. M., Polymer Spherulites: A Critical Review. *Prog. Polym. Sci.* **2016**, *56*, 1-63.
- (2) Prud'homme, R. E., Crystallization and morphology of ultrathin films of homopolymers and polymer blends. *Prog. Polym. Sci.* **2016**, *54-55*, 214-231.
- (3) Liu, Y.-X.; Chen, E.-Q., Polymer crystallization of ultrathin films on solid substrates. *Coord.*

Chem. Rev. **2010**, *254* (9-10), 1011-1037.

(4) Taguchi, K.; Miyaji, H.; Izumi, K.; Hoshino, A.; Miyamoto, Y.; Kokawa, R., Crystal Growth of Isotactic Polystyrene in Ultrathin Films: Film Thickness Dependence. *J. Macromol. Sci., Part B* **2002**, *41* (4-6), 1033-1042.

(5) Reiter, G.; Sommer, J.-U., Polymer Crystallization in Quasi-2 Dimensions. I. Experimental Results. *J. Chem. Phys.* **2000**, *112* (9), 4376-4383.

(6) Mareau, V. H.; Prud'Homme, R. E., In-situ Hot Stage Atomic Force Microscopy Study of Poly (ϵ -caprolactone) Crystal Growth in Ultrathin Films. *Macromolecules* **2005**, *38* (2), 398-408.

(7) Wang, Y.; Rafailovich, M.; Sokolov, J.; Gersappe, D.; Araki, T.; Zou, Y.; Kilcoyne, A.; Ade, H.; Marom, G.; Lustiger, A., Substrate Effect on the Melting Temperature of Thin Polyethylene Films. *Phys. Rev. Lett.* **2006**, *96* (2), 028303.

(8) Wang, Y.; Chan, C.-M.; Ng, K.-M.; Li, L., What Controls the Lamellar Orientation at the Surface of Polymer Films during Crystallization? *Macromolecules* **2008**, *41* (7), 2548-2553.

(9) Lotz, B.; Miyoshi, T.; Cheng, S. Z., 50th Anniversary Perspective: Polymer Crystals and Crystallization: Personal Journeys in a Challenging Research Field. *Macromolecules* **2017**, *50* (16), 5995-6025.

(10) Statz, A. R.; Meagher, R. J.; Barron, A. E.; Messersmith, P. B., New Peptidomimetic Polymers for Antifouling Surfaces. *J. Am. Chem. Soc.* **2005**, *127* (22), 7972-7973.

(11) Statz, A. R.; Barron, A. E.; Messersmith, P. B., Protein, Cell and Bacterial Fouling Resistance of Polypeptoid-Modified Surfaces: Effect of Side-Chain Chemistry. *Soft Matter* **2008**, *4* (1), 131-139.

(12) Lau, K. H.; Ren, C.; Sileika, T. S.; Park, S. H.; Szleifer, I.; Messersmith, P. B., Surface-Grafted polysarcosine as a peptoid antifouling polymer brush. *Langmuir* **2012**, *28* (46), 16099-16107.

(13) Li, A.; Zhang, D., Synthesis and Characterization of Cleavable Core-Cross-Linked Micelles Based on Amphiphilic Block Copolypeptoids as Smart Drug Carriers. *Biomacromolecules* **2016**, *17* (3), 852-861.

(14) Zhu, L.; Simpson, J. M.; Xu, X.; He, H.; Zhang, D.; Yin, L., Cationic Polypeptoids with Optimized Molecular Characteristics toward Efficient Nonviral Gene Delivery. *ACS Appl. Mater. Interfaces* **2017**, *9* (28), 23476-23486.

(15) Luo, Y.; Song, Y.; Wang, M.; Jian, T.; Ding, S.; Mu, P.; Liao, Z.; Shi, Q.; Cai, X.; Jin, H.; Du, D.; Dong, W. J.; Chen, C. L.; Lin, Y., Bioinspired Peptoid Nanotubes for Targeted Tumor Cell Imaging and Chemo-Photodynamic Therapy. *Small* **2019**, *15* (43), 1902485.

(16) Murray, D. J.; Kim, J. H.; Grzincic, E. M.; Kim, S. C.; Abate, A. R.; Zuckermann, R. N., Uniform, Large-Area, Highly Ordered Peptoid Monolayer and Bilayer Films for Sensing Applications. *Langmuir* **2019**, *35* (42), 13671-13680.

(17) Tao, X.; Chen, H.; Trepout, S.; Cen, J.; Ling, J.; Li, M. H., Polymersomes with Aggregation-Induced Emission based on Amphiphilic Block Copolypeptoids. *Chem. Commun.* **2019**, *55* (90), 13530-13533.

(18) Chan, B. A.; Xuan, S.; Li, A.; Simpson, J. M.; Sternhagen, G. L.; Yu, T.; Darvish, O. A.; Jiang, N.; Zhang, D., Polypeptoid Polymers: Synthesis, Characterization, and Properties. *Biopolymers* **2018**, *109* (1), 23070.

(19) Xuan, S.; Zuckermann, R. N., Diblock Copolypeptoids: A Review of Phase Separation,

Crystallization, Self-Assembly and Biological Applications. *J. Mater. Chem. B* **2020**, *8* (25), 5380-5394.

(20) Lee, C.-U.; Smart, T. P.; Guo, L.; Epps, T. H.; Zhang, D., Synthesis and Characterization of Amphiphilic Cyclic Diblock Copolypeptoids from N-Heterocyclic Carbene-Mediated Zwitterionic Polymerization of N-Substituted N-Carboxyanhydride. *Macromolecules* **2011**, *44* (24), 9574-9585.

(21) Cha, Y.; Jarrett-Wilkins, C.; Rahman, M. A.; Zhu, T.; Sha, Y.; Manners, I.; Tang, C., Crystallization-Driven Self-Assembly of Metallo-Polyelectrolyte Block Copolymers with a Polycaprolactone Core-Forming Segment. *ACS Macro Lett.* **2019**, *8* (7), 835-840.

(22) Jiang, N.; Yu, T.; Darvish, O. A.; Qian, S.; Mkam Tsengam, I. K.; John, V.; Zhang, D., Crystallization-Driven Self-Assembly of Coil-Comb-Shaped Polypeptoid Block Copolymers: Solution Morphology and Self-Assembly Pathways. *Macromolecules* **2019**, *52* (22), 8867-8877.

(23) Sun, J.; Jiang, X.; Lund, R.; Downing, K. H.; Balsara, N. P.; Zuckermann, R. N., Self-assembly of Crystalline Nanotubes from Monodisperse Amphiphilic Diblock Copolypeptoid Tiles. *Proc. Natl. Acad. Sci. U.S.A.* **2016**, *113* (15), 3954-3959.

(24) Jiang, X.; Greer, D. R.; Kundu, J.; Ophus, C.; Minor, A. M.; Prendergast, D.; Zuckermann, R. N.; Balsara, N. P.; Downing, K. H., Imaging Unstained Synthetic Polymer Crystals and Defects on Atomic Length Scales Using Cryogenic Electron Microscopy. *Macromolecules* **2018**, *51* (19), 7794-7799.

(25) Kang, L.; Chao, A.; Zhang, M.; Yu, T.; Wang, J.; Wang, Q.; Yu, H.; Jiang, N.; Zhang, D., Modulating the Molecular Geometry and Solution Self-Assembly of Amphiphilic Polypeptoid Block Copolymers by Side Chain Branching Pattern. *J. Am. Chem. Soc.* **2021**, *143* (15), 5890-5902.

(26) Shi, Z.; Wei, Y.; Zhu, C.; Sun, J.; Li, Z., Crystallization-Driven Two-Dimensional Nanosheet from Hierarchical Self-Assembly of Polypeptoid-Based Diblock Copolymers. *Macromolecules* **2018**, *51* (16), 6344-6351.

(27) Sun, J.; Wang, Z.; Zhu, C.; Wang, M.; Shi, Z.; Wei, Y.; Fu, X.; Chen, X.; Zuckermann, R. N., Hierarchical Supramolecular Assembly of a Single Peptoid Polymer into a Planar Nanobrush with Two Distinct Molecular Packing Motifs. *Proc. Natl. Acad. Sci. U.S.A.* **2020**, *117* (50), 31639-31647.

(28) Lee, C.-U.; Li, A.; Ghale, K.; Zhang, D., Crystallization and Melting Behaviors of Cyclic and Linear Polypeptoids with Alkyl Side Chains. *Macromolecules* **2013**, *46* (20), 8213-8223.

(29) Greer, D. R.; Stolberg, M. A.; Xuan, S.; Jiang, X.; Balsara, N. P.; Zuckermann, R. N., Liquid-Crystalline Phase Behavior in Polypeptoid Diblock Copolymers. *Macromolecules* **2018**, *51* (23), 9519-9525.

(30) Greer, D. R.; Stolberg, M. A.; Kundu, J.; Spencer, R. K.; Pascal, T.; Prendergast, D.; Balsara, N. P.; Zuckermann, R. N., Universal Relationship between Molecular Structure and Crystal Structure in Peptoid Polymers and Prevalence of the cis Backbone Conformation. *J. Am. Chem. Soc.* **2018**, *140* (2), 827-833.

(31) Wang, Y.; Ge, S.; Rafailovich, M.; Sokolov, J.; Zou, Y.; Ade, H.; Lüning, J.; Lustiger, A.; Maron, G., Crystallization in the Thin and Ultrathin Films of Poly (ethylene-vinyl acetate) and Linear Low-Density Polyethylene. *Macromolecules* **2004**, *37* (9), 3319-3327.

(32) Jiang, N.; Chen, J.; Yu, T.; Chao, A.; Kang, L.; Wu, Y.; Niu, K.; Li, R.; Fukuto, M.; Zhang, D., Cyclic Topology Enhancing Structural Ordering and Stability of Comb-Shaped Polypeptoid Thin

Films against Melt-Induced Dewetting. *Macromolecules* **2020**, *53* (17), 7601-7612.

(33) Scherrer, P., Bestimmung Der Inneren Struktur und der Größe von Kolloidteilchen Mittels Röntgenstrahlen. In *Kolloidchemie Ein Lehrbuch*, Zsigmondy, R., Ed. Springer Berlin Heidelberg: Berlin, Heidelberg, 1912; pp 387-409.

(34) Hsu, C. H.; Dong, X. H.; Lin, Z.; Ni, B.; Lu, P.; Jiang, Z.; Tian, D.; Shi, A. C.; Thomas, E. L.; Cheng, S. Z., Tunable Affinity and Molecular Architecture Lead to Diverse Self-Assembled Supramolecular Structures in Thin Films. *ACS Nano* **2016**, *10* (1), 919-929.

(35) Knaapila, M.; Lyons, B. P.; Kisko, K.; Foreman, J. P.; Vainio, U.; Mihaylova, M.; Seeck, O. H.; Pålsson, L.-O.; Serimaa, R.; Torkkeli, M.; Monkman, A. P., X-ray Diffraction Studies of Multiple Orientation in Poly(9,9-bis(2-ethylhexyl)fluorene-2,7-diyl) Thin Films. *J. Phys. Chem. B* **2003**, *107* (45), 12425-12430.

(36) Lee, B.; Park, I.; Yoon, J.; Park, S.; Kim, J.; Kim, K.-W.; Chang, T.; Ree, M., Structural Analysis of Block Copolymer Thin Films with Grazing Incidence Small-Angle X-ray Scattering. *Macromolecules* **2005**, *38* (10), 4311-4323.

(37) Ho, V.; Boudouris, B. W.; Segalman, R. A., Tuning Polythiophene Crystallization through Systematic Side Chain Functionalization. *Macromolecules* **2010**, *43* (19), 7895-7899.

(38) Beckingham, B. S.; Ho, V.; Segalman, R. A., Melting Behavior of Poly(3-(2'-ethyl)hexylthiophene). *Macromolecules* **2014**, *47* (23), 8305-8310.

(39) Davidson, E. C.; Segalman, R. A., Confined Crystallization within Cylindrical P3EHT Block Copolymer Microdomains. *Macromolecules* **2017**, *50* (16), 6128-6136.

(40) Brinkmann, M.; Charoenthai, N.; Traiphol, R.; Piyakulawat, P.; Wlosnewski, J.; Asawapirom, U., Structure and Morphology in Highly Oriented Films of Poly(9,9-bis(n-octyl)fluorene-2,7-diyl) and Poly(9,9-bis(2-ethylhexyl)fluorene-2,7-diyl) Grown on Friction Transferred Poly(tetrafluoroethylene). *Macromolecules* **2009**, *42* (21), 8298-8306.

(41) Wunderlich, B., *Macromolecular Physics, Volume 2: Crystal Nucleation, Growth, Annealing*. Academic Press: New York and London, 1976.

(42) Li, L.; Chan, C.-M.; Yeung, K. L.; Li, J.-X.; Ng, K.-M.; Lei, Y., Direct Observation of Growth of Lamellae and Spherulites of a Semicrystalline Polymer by AFM. *Macromolecules* **2001**, *34* (2), 316-325.

